

# 1 **Identification of BBOX1 as a Therapeutic Target in Triple-Negative Breast Cancer**

2 Chengheng Liao<sup>1</sup>, Yang Zhang<sup>2</sup>, Cheng Fan<sup>3</sup>, Laura E. Herring<sup>4</sup>, Juan Liu<sup>5</sup>, Jason W. Locasale<sup>5</sup>,  
3 Mamoru Takada<sup>6</sup>, Jin Zhou<sup>1</sup>, Giada Zurlo<sup>1</sup>, Lianxin Hu<sup>1</sup>, Jeremy M. Simon<sup>3,7,8</sup>, Travis S.  
4 Ptacek<sup>3,8</sup>, Victor G. Andrianov<sup>9</sup>, Einars Loza<sup>9</sup>, Yan Peng<sup>1</sup>, Huanghe Yang<sup>2</sup>, Charles M. Perou<sup>3</sup>,  
5 and Qing Zhang<sup>1</sup>

6 <sup>1</sup> Department of Pathology, University of Texas Southwestern Medical Center, Dallas, TX 75390,  
7 USA

8 <sup>2</sup> Department of Biochemistry, Duke University, Durham, NC 27710

9 <sup>3</sup> Lineberger Comprehensive Cancer Center, University of North Carolina School of Medicine,  
10 Chapel Hill, NC 27599, USA

11 <sup>4</sup> Department of Pharmacology and UNC Proteomics Core Facility, University of North Carolina,  
12 Chapel Hill, NC 27599, USA

13 <sup>5</sup> Department of Pharmacology and Cancer Biology, Duke University School of Medicine,  
14 Durham, NC 27710, USA.

15 <sup>6</sup> Department of General Surgery, Chiba University Graduate School of Medicine, 1-8-1,  
16 Inohana, Chuoku, Chiba, 260-0856, Japan

17 <sup>7</sup> Department of Genetics, Neuroscience Center, University of North Carolina, Chapel Hill, NC  
18 27599, USA

19 <sup>8</sup> UNC Neuroscience Center, Carolina Institute for Developmental Disabilities, University of  
20 North Carolina, Chapel Hill, NC 27599, USA

21 <sup>9</sup> Latvian Institute of Organic Synthesis, 21 Aizkraukles street, LV1006, Riga, Latvia

22 **Running title:** BBOX1 is a novel therapeutic target in TNBC

23 **Keywords:** TNBC, 2-OG-dependent dioxygenases, BBOX1, IP3R3, Calcium signaling

24 **Financial support:** This work was supported by Cancer Prevention and Research Institute of  
25 Texas (Q. Zhang, CPRIT, RR190058), NCI Breast SPORE program (C.M. Perou, P50-  
26 CA58223), National Cancer Institute (C.M. Perou, R01-CA148761) and BCRF (C.M. Perou).

27 **Conflict of interests:** C.M.P is an equity stock holder and consultant of BioClassifier LLC;

28 C.M.P is also listed an inventor on patent applications on the Breast PAM50 Subtyping assay.

29 Corresponding author (Q.Z): [Qing.Zhang@UTSouthwestern.edu](mailto:Qing.Zhang@UTSouthwestern.edu)

30 Qing Zhang, Ph.D. Associate Professor

31 Department of Pathology

32 UT Southwestern Medical Center

33 5323 Harry Hines Blvd., NB7.208

34 Dallas, Texas 75390-9072

35 Tel: 214-645-4671

36 Fax: 214-648-1102

37 **ABSTRACT**

38 Triple-negative breast cancer (TNBC) is an aggressive and highly lethal disease. Due to its  
39 heterogeneity and lack of hormone receptors or HER2 expression, targeted therapy is limited.  
40 Here, by performing a functional siRNA screening for 2-OG-dependent enzymes, we identified  
41 gamma-butyrobetaine hydroxylase 1 (BBOX1) as an essential gene for TNBC tumorigenesis.  
42 BBOX1 depletion inhibits TNBC cell growth, while not affecting normal breast cells.  
43 Mechanistically, BBOX1 binds with the calcium channel inositol-1,4,5-trisphosphate receptor  
44 type 3 (IP3R3) in an enzymatic-dependent manner and prevents its ubiquitination and  
45 proteasomal degradation. BBOX1 depletion suppresses IP3R3 mediated endoplasmic reticulum  
46 calcium release, therefore impairing calcium-dependent energy-generating processes including  
47 mitochondrial respiration and mTORC1 mediated glycolysis, which leads to apoptosis and  
48 impaired cell cycle progression in TNBC cells. Therapeutically, genetic depletion or  
49 pharmacological inhibition of BBOX1 inhibits TNBC tumor growth *in vitro* and *in vivo*. Our study  
50 highlights the importance of targeting previously uncharacterized BBOX1-IP3R3-calcium  
51 oncogenic signaling axis in TNBC.

52

53 **SIGNIFICANCE**

54 We provide evidence from unbiased screens that BBOX1 is a potential therapeutic target in  
55 TNBC and genetic knockdown or pharmacological inhibition of BBOX1 leads to decreased  
56 TNBC cell fitness. This study lays the foundation for developing effective BBOX1 inhibitors for  
57 treatment of this lethal disease.

58

59

## 60 INTRODUCTION

61 Triple-negative breast cancer (TNBC) is a highly heterogeneous and clinically aggressive  
62 disease that accounts for 15-20% of breast cancers, causing the highest mortality rate among  
63 all breast cancer subtypes (1,2). TNBC is an immunohistochemically-defined subtype of breast  
64 cancer that does not express estrogen receptor (ER) and progesterone receptor (PR)  
65 expression, and lack human epidermal growth factor receptor 2 (*HER2*) amplification. In  
66 contrary to hormone receptor positive breast cancer which is commonly fought with endocrine  
67 therapy or *HER2* positive breast cancer that can be treated by therapeutic antibodies (e.g.  
68 Trastuzumab), TNBC has no targeted therapy and conventional chemotherapy remains the  
69 standard of care for patients with TNBC (3). Therefore, the identification of novel targets with  
70 actionable therapeutic drugs that specially targeting TNBC vulnerabilities could greatly benefit  
71 the clinical outcome of TNBC patients.

72 2-oxoglutarate (2-OG)-dependent enzymes, which use oxygen and 2-OG as co-  
73 substrates and Fe(II) as a cofactor, catalyze various cellular biological enzymatic reactions with  
74 a broad spectrum of substrates (e.g. DNA, RNA, and proteins) (4). Emerging literature indicates  
75 that they also play important roles in various malignant diseases. For example, the function of  
76 ten-eleven translocation (TET) DNA hydroxylases has been well documented in hematological  
77 malignancies (4). Prolyl hydroxylases regulate cancer cell growth by modulating the level of  
78 their substrates including hypoxia-inducible factors alpha ( $HIF\alpha s$ ) and forkhead box O3a  
79 (FOXO3a) (5,6). Histone demethylases, by modulating methylation of some histone residues  
80 including H3K4 and H3K36, regulate gene expression that has been linked to the pathogenesis  
81 of several cancers (7,8). Our recent studies suggested that the hydroxylase EglN2 and its  
82 downstream substrate adenylosuccinate lyase (ADSL) positively contribute to TNBC  
83 tumorigenesis (9,10). These studies indicate that the dysfunction of 2-OG dependent enzymes  
84 may associate with various cancers including breast cancer. However, there lacks a systematic  
85 approach to unbiasedly screen for critical enzymes that contribute to TNBC progression.

86 In the present study, we sought to identify novel therapeutic targets in TNBC among 2-  
87 OG dependent enzymes through an unbiased siRNA library screening, with the gene depletion  
88 affecting cell growth both in 2-D cell proliferation and 3-D anchorage-independent growth. We  
89 show that gamma-butyrobetaine hydroxylase 1 (BBOX1), a member of 2-OG dependent  
90 enzyme catalyzing the carnitine biosynthesis (11) that has never been characterized in cancers,  
91 is important for TNBC progression. We aim to characterize the oncogenic function of BBOX1,  
92 elucidate the molecular mechanism by which BBOX1 contributes to TNBC and explore its  
93 therapeutic potential in relevant TNBC models.

94

## 95 **RESULTS**

### 96 **Identification of BBOX1 as an Essential Gene for TNBC Cell Growth**

97 To identify potential novel 2-OG-dependent enzymes that may contribute to TNBC cell  
98 growth, we obtained an on-target plus siRNA library that targets all the members of family  
99 enzymes (**Supplementary Table S1**). We developed a screening method that examines both 2-  
100 D MTS cell proliferation and 3-D anchorage-independent growth with a representative TNBC  
101 cell line MDA-MB-231 (**Supplementary Fig. S1A**). In addition, we included several independent  
102 siRNAs for the house-keeping gene glyceraldehyde 3-phosphate dehydrogenase (GAPDH)  
103 which scored among the top hits from the screening (**Fig. 1A**). We identified nine enzymes that  
104 scored both in the 2-D and 3-D screening, showing significant growth defect upon gene  
105 depletion by siRNAs (**Fig. 1B and C; Supplementary Fig. S1B**). Among them, jumonji domain-  
106 containing protein 6 (JMJD6), lysine demethylase 6A (KDM6A) have been previously identified  
107 to be important for maintaining MDA-MB-231 cell growth (12,13). Among other positive hits from  
108 our screening, AlkB Homolog 4 lysine demethylase (ALKBH4) depletion led to decreased cell  
109 proliferation in MDA-MB-231 cells but also in the immortalized normal breast epithelial cell line  
110 HMLE (**Supplementary Fig. S1C and S1D**), suggesting that ALKBH4 may be an essential  
111 gene for both normal and breast cancer cell survival. Interestingly, two enzymes involved in

112 carnitine synthesis, gamma-butyrobetaine hydroxylase 1 (BBOX1) and trimethyllysine  
113 hydroxylase epsilon (TMLHE), were found to be critical of TNBC cell growth, suggesting the  
114 importance of this pathway in TNBC. We tested either BBOX1/TMLHE deletion alone or in  
115 combination in MDA-MB-231 cell and found no significant additive effect on cell proliferation or  
116 soft agar growth with co-deletion compared to either gene deletion (**Supplementary Fig. S1E–**  
117 **S1H**). Since BBOX1 acts downstream of TMLHE in the carnitine synthesis pathway, we decided  
118 to focus on the characterization of BBOX1 in TNBC. Indeed, BBOX1 was found to be essential  
119 for the growth of multiple TNBC cells (MDA-MB-231, 436 and 468) (**Fig. 1D and E;**  
120 **Supplementary Fig. S1I**), but not for the normal breast epithelial cell line as verified by two  
121 individual siRNAs (**Supplementary Fig. S1J–S1L**).

122 Our screening data suggest that BBOX1 may be a novel oncogene in TNBC. We  
123 examined BBOX1 protein levels in a panel of breast cancer cell lines and found that BBOX1  
124 expression was generally higher in basal-like breast cancer cell lines compared to other  
125 subtypes of breast cancer cells or normal breast epithelial cells (**Fig. 1F**). In the breast cancer  
126 patient datasets TCGA, METABRIC and UNC337 (14-16), BBOX1 expression was the highest  
127 in basal-like breast cancer patients, where most of TNBC patients belong (17) (**Fig. 1G**). In  
128 addition, higher expression of BBOX1 predicted worse prognosis only in basal-like TNBC  
129 patients, but not in luminal A, B or Her2<sup>+</sup> breast cancer patients (**Fig. 1H**).

130 In line with the results obtained with siRNAs, BBOX1 depletion by shRNAs induced a  
131 growth deficient phenotype in both 2-D MTS assay and colony formation, as well as 3-D soft  
132 agar in TNBC cells, including MDA-MB-468, HCC70, and HCC3153 (**Fig. 2A–2C;**  
133 **Supplementary Fig. S2A**). BBOX1 depletion in BT474, a BBOX1-high expressing HER2<sup>+</sup> cell  
134 line (**Fig. 1F**), also caused similar growth defect phenomenon (**Fig. 2A–2C; Supplementary**  
135 **Fig. S2A**). However, BBOX1 depletion in the BBOX1-low expressing breast cancer cell lines  
136 (MCF-7 and T47D), or normal breast epithelial cell lines (MCF-10A and HMLE) did not cause an

137 overt effect on cell proliferation (**Fig. 2A–2C; Supplementary Fig. S2B**). Collectively, these  
138 data show that BBOX1 depletion caused cell proliferation defect preferentially in TNBC cells.  
139 However, its knockdown could also lead to growth defect in other subtypes of breast cancer  
140 cells displaying high BBOX1 protein levels.

141

## 142 **BBOX1 Promotes TNBC Cell Growth in an Enzymatic-Dependent Fashion**

143 Next, we aimed to examine whether BBOX1 overexpression induces TNBC cell  
144 proliferation and, if so, whether this phenotype is mediated by its enzymatic activity. First, we  
145 found that overexpression of BBOX1 promotes the 2-D or 3-D cell growth in MDA-MB-436,  
146 SUM149, MCF-10A and HMLE (**Supplementary Fig. S2C–S2G**). We then infected MDA-MB-  
147 231, 436 and 468 cells with vector, wild type (WT) or catalytically inactive mutant (N2D) BBOX1  
148 by double mutating the two key amino acid residues (Asn191, Asn292) which are critical for  
149 substrate  $\gamma$ -butyrobetaine (GBB) binding (18). In these cell lines, we observed increased cell  
150 proliferation with WT BBOX1 overexpression, the phenotype not observed with BBOX1-N2D  
151 mutant expression despite that WT and N2D BBOX1 had similar expression (**Fig. 2D and E;**  
152 **Supplementary Fig. S2H–S2K**). Next, we depleted endogenous BBOX1 from MDA-MB-468  
153 cells followed by the restoration of either shRNA-resistant WT BBOX1 or N2D (**Fig. 2F**). WT  
154 BBOX1, but not BBOX1-N2D, efficiently rescued the growth defect in cell proliferation, 2-D  
155 colony growth and 3-D soft agar growth induced by BBOX1 depletion in these cells (**Fig. 2G–2I**).  
156 Our results suggest that BBOX1 promotes TNBC cell growth in an enzymatic-dependent  
157 manner.

158 BBOX1 is a critical enzyme involved in carnitine synthesis (19). Carnitine is essential for  
159 lipid metabolism by transporting long-chain fatty acids into the mitochondria for  $\beta$ -oxidation (20).  
160 We ask whether BBOX1 regulates TNBC cell growth through carnitine synthesis. To this end,  
161 we performed a metabolomics study in MDA-MB-468 cells. Over 300 metabolites were detected  
162 in these cells with ~130 metabolites that were decreased ( $P < 0.05$ ) in BBOX1 KD (**Fig. 2J**). We

163 then conducted metabolic pathway analysis (21) and found that BBOX1 depletion affected the  
164 carnitine synthesis pathway (**Fig. 2K**), which was also confirmed by modest but statistically  
165 significant carnitine level decrease upon BBOX1 KD in TNBC cells (**Fig. 2L**). To examine the  
166 function of carnitine in TNBC cells, we supplied the MDA-MB-468 shRNA control or BBOX1 KD  
167 cells with carnitine and palmitate in fatty acids free condition medium and measured the  
168 mitochondrial oxygen consumption rate (OCR) as an indicator of exogenous fatty acid oxidation  
169 (FAO). Indeed, the carnitine supplement took effect on utilizing palmitate to promote OCR in  
170 MDA-MB-468 cells (**Supplementary Fig. S2L**). However, we found that the FAO based OCR  
171 rate in BBOX1 KD cells is still lower than the control cells (**Fig. 2M**), indicating that carnitine is  
172 not sufficient to rescue the defect of OCR in BBOX1 KD cells. In addition, the carnitine  
173 supplement failed to rescue the growth defect of MDA-MB-468 BBOX1 depleted cells (**Fig. 2N**).  
174 Collectively, these data show that BBOX1 promotes TNBC cell growth via its catalytic activity  
175 while independent of carnitine biosynthesis.

176

### 177 **BBOX1 Controls IP3R3 Protein Stability in TNBC**

178 To understand the potential molecular mechanism of BBOX1 positive regulation of  
179 TNBC cell proliferation, we performed TAP-TAG purification followed by mass spectrometry in  
180 MDA-MB-231 expressing either empty vector (EV), WT or N2D BBOX1 to identify the BBOX1-  
181 binding proteins in each of these conditions (**Fig. 3A**). Whereas an equal number of BBOX1  
182 peptides were retrieved from both WT and catalytically dead N2D, inositol 1,4,5-trisphosphate  
183 receptor type 3 (IP3R3) was the top hit with the most peptides detected in the WT BBOX1, but  
184 not in the EV- or BBOX1-N2D-expressing cells (**Fig. 3B**), suggesting that IP3R3 is a unique  
185 BBOX1 binding partner and its binding depends on BBOX1 enzymatic activity. IP3R3 is an  
186 important endoplasmic reticulum (ER) calcium channel for the control of intracellular calcium  
187 release from the ER into the mitochondria (22). Emerging literature has highlighted IP3R3 as  
188 the specific gene among the three close family members (IP3R1, IP3R2, and IP3R3)

189 contributing to malignancy in multiple cancers, including breast cancer (23-26). Co-  
190 immunoprecipitations (co-IPs) in multiple TNBC cell lines further confirmed the binding of IP3R3  
191 to WT BBOX1, but not catalytically N2D mutant (**Fig. 3C; Supplementary Fig. S3A and S3B**).  
192 Importantly, we also observed this interaction in a physiological setting, showing that the  
193 endogenous BBOX1 could bind with endogenous IP3R3 in TNBC cell lines including HCC70  
194 and MDA-MB-468 (**Fig. 3D; Supplementary Fig. S3C**).

195 IP3R3 encodes a protein that harbors 2670 amino acids, which makes the expression of  
196 full-length constructs challenging. To investigate the potential domain on IP3R3 that may bind  
197 with BBOX1, we obtained a series of IP3R3 truncation mutants (1-226 aa, 227-800 aa, 801-  
198 2230 aa and 2180-2670 aa) as published previously (**Supplementary Fig. S3D**) (27) and found  
199 that the amino acid sequence spanning from 227-800 was the major domain responsible for the  
200 binding with BBOX1 (**Supplementary Fig. S3E**). We also obtained two additional truncation  
201 mutants (232-436 and 436-587 aa) and found that the region containing 232-436 amino acids  
202 bound to BBOX1 (**Supplementary Fig. S3F**).

203 Previous research showed that the IP3R3 amino acid sequence between 227-602 was  
204 mainly responsible for its binding with the E3 ubiquitin ligase f-box and leucine rich repeat  
205 protein 2 (FBXL2) followed by its ubiquitination and degradation (27). Interestingly, in our  
206 system, we found that FBXL2 interacts with the IP3R3 region located between amino acids 232-  
207 587, which covers the same region bound by BBOX1 (**Supplementary Fig. S3G**). Therefore,  
208 we speculated that BBOX1 might bind with IP3R3 and affect its protein stability. To test this, we  
209 first examined the protein levels of IP3R3 upon BBOX1 knockdown in multiple TNBC cell lines.  
210 BBOX1 depletion, which mediated by shRNAs, led to decreased IP3R3 protein level in these  
211 cell lines, whereas leaving the other two homologs IP3R1 and IP3R2 unaffected (**Fig. 3E**). In  
212 support of this finding, doxycycline-induced BBOX1 depletion also led to decreased IP3R3  
213 protein levels (**Fig. 3F**). This phenotype could be rescued by co-treatment of these BBOX1-  
214 depleted cells with the proteasomal inhibitor MG132 or the neddylation inhibitor MLN4924 (28)

215 **(Fig. 3G; Supplementary Fig. S4A)**, suggesting that IP3R3 is subjected to ubiquitination-  
216 mediated proteasomal degradation and its protein stability is regulated by BBOX1. Consistently,  
217 BBOX1 depletion led to increased IP3R3 ubiquitination, which corresponded to decreased  
218 IP3R3 protein levels in these cells **(Fig. 3H)**. We also performed pulse chase experiments with  
219 cycloheximide (CHX) to inhibit new protein synthesis and found that BBOX1 depletion led to  
220 decreased IP3R3 protein stability **(Fig. 3I; Supplementary Fig. S4B and S4C)**. Since IP3R3  
221 protein was previously shown to be degraded by FBXL2 E3 ligase (27) and we recapitulated the  
222 phenomenon in TNBC cells **(Fig. 3J)**, we pursued to determine whether BBOX1 might affect the  
223 binding between FBXL2 and IP3R3. First, we overexpressed different dosages of BBOX1 and  
224 found that increased WT, but not catalytically dead, BBOX1 expression correlated with  
225 decreased binding of FBXL2 and IP3R3, corresponding with decreased IP3R3 ubiquitination  
226 **(Fig. 3K and L; Supplementary Fig. S4D)**. In accordance with this finding, WT BBOX1, but not  
227 BBOX1-N2D, rescued the protein levels of IP3R3 regulated by BBOX1 depletion by both  
228 shRNAs **(Fig. 3M; Supplementary Fig. S4E)**. Overexpression of the WT BBOX1, but not the  
229 N2D mutant, increased IP3R3 protein level in multiple breast cancer cell lines or normal  
230 epithelial cells **(Supplementary Fig. S4F)**. In accordance with the regulation of BBOX1 on  
231 IP3R3, IP3R3 and BBOX1 protein levels also showed similar expression patterns in these  
232 basal-like TNBC cells **(Fig. 3N)**. Interestingly, BBOX1 and IP3R3 protein level did not correlate  
233 well in claudin-low MDA-MB-231 cells **(Fig. 3N)**, which suggests other layers of regulation on  
234 IP3R3 exists in this cell, such as PTEN as previously published (27). To further examine the  
235 clinical relevance of BBOX1 expression in breast cancer patients, we stained two different  
236 commercially available breast cancer tissue microarray (TMA) datasets containing all breast  
237 cancer subtypes with BBOX1 as well as IP3R3, followed by the quantification of signal  
238 intensities. H score was used to determine the immunohistochemistry staining intensities with  
239 these two proteins and was divided into four grades (I-IV) based on the staining intensity (29).  
240 IP3R3 protein expression level correlated strongly with BBOX1 in these breast cancer TMAs

241 **(Fig. 3O and P; Supplementary Fig. S4G and S4H)**, suggesting the clinical relevance of  
242 BBOX1-IP3R3 in breast cancer patients. In conclusion, our results show that BBOX1 binds with  
243 IP3R3 in an enzymatic-dependent manner and protects IP3R3 from FBXL2-mediated  
244 ubiquitination and degradation.

245

### 246 **BBOX1-IP3R3-Calcium Signaling Sustains Mitochondrial Activity and mTORC1-** 247 **dependent Glycolysis that is Required for TNBC Cell Growth and Survival**

248 Next, we sought to examine the biological function of BBOX1-mediated IP3R3 regulation  
249 in TNBC cells. Previous study reported that constitutive IP3R3-mediated calcium release is  
250 required for maintaining cellular bioenergetics, contributing to sustained mitochondrial function  
251 and eventually cell proliferation (30). Since BBOX1 depletion led to decreased IP3R3 protein  
252 levels (**Fig. 3E and F**), we first examined the effect of BBOX1 on ER calcium release. We found  
253 that the ATP-induced intracellular calcium elevation in TNBC cells is mainly obtained through  
254 IP3R3-mediated ER calcium release because 1) calcium influx through the plasma membrane  
255 was prevented by the absence of extracellular calcium; 2) knockdown of IP3R3 essentially  
256 eliminated ATP-induced calcium responses (27,31) (**Fig. 4A**). Notably, ATP-induced ER calcium  
257 release was significantly reduced when knocking down BBOX1 compared to the control (**Fig.**  
258 **4A; Supplementary Fig. S5A**). Next, we investigated whether BBOX1 mediated calcium  
259 release could affect mitochondrial function. We first showed that in the MDA-MB-468 and  
260 HCC70 but not MCF-10A cells, depletion of IP3R3 significantly decreases OCR as an indication  
261 of mitochondrial activity (**Fig. 4B and C; Supplementary Fig. S5B and S5C**) which is  
262 consistent with the previous report (30). BBOX1 depletion also led to decreased OCR in MDA-  
263 MB-468 and HCC70 cells (**Fig. 4D**), the phenotype rescued by WT but not the N2D catalytic  
264 mutant BBOX1 (**Supplementary Fig. S5D and S5E**). Moreover, the metabolomics pathway  
265 analysis (**Fig. 2K**) show that the TCA cycle related metabolites, such as citrate, ATP and NADH,  
266 decreased upon BBOX1 depletion (**Fig. 4E; Supplementary Fig. S5F**). Despite the comparable

267 BBOX1 knockdown with two hairpins, metabolomics showed that BBOX1 sh2 displayed more  
268 robust effect than sh1, which remains to be investigated.

269 Interestingly, besides the TCA cycle, we observed that some other important metabolic  
270 pathways were also enriched in the metabolomics analysis, such as the Warburg Effect (aerobic  
271 glycolysis) and pyrimidine metabolism (**Fig. 2K**), which are frequently altered or reprogrammed  
272 in cancer cells (32,33). The glycolysis pathway was also suppressed with decreased glycolytic  
273 metabolites and increased glucose (**Supplementary Fig. S5F and S5G**). In order to understand  
274 how BBOX1 depletion may affect the metabolic changes we observed, we performed BBOX1  
275 gene expression profiling by RNA-seq and gene set enrichment analysis (GSEA) showed that  
276 the glycolysis pathway was enriched in control cells compared to BBOX1 depleted MDA-MB-  
277 468 cells (**Fig. 4F and G; Supplementary Fig. S6A**). Interestingly, we also noted that the  
278 mTORC1 pathway, a key regulator of glycolysis in cancer cells (34,35), was enriched in our  
279 GSEA analysis (**Fig. 4F and G; Supplementary Fig. S6B**), suggesting the suppression of  
280 mTORC1 might account for the impaired glycolysis in BBOX1 KD cells.

281 Next, we sought to address how mTORC1 is affected upon BBOX1 depletion. Notably,  
282 there is emerging literature indicating that cytosolic calcium is required for mTORC1 activation  
283 (36-38). Firstly we checked the mTORC1 activity by western blot upon IP3R3 depletion. As  
284 shown by mTORC1 mediated S6 kinase 1 (S6K1) Thr389 phosphorylation and the subsequent  
285 S6 Ser240/244 phosphorylation, mTORC1 activity was abolished when IP3R3 was depleted in  
286 MDA-MB-468 cells (**Fig. 4H**). We also observed modest but consistent mTORC1 activity  
287 downregulation by knocking down BBOX1 in MDA-MB-468 and HCC70 (**Fig. 4I;**  
288 **Supplementary Fig. S6C**). To further validate that calcium is required for mTORC1 activation in  
289 TNBC, we treated the BBOX1 KD cells with the ER Ca<sup>2+</sup>-ATPase inhibitor thapsigargin (Tg)  
290 which causes a rapid increase of cytosolic calcium (39), or co-treated them with Tg and the  
291 calcium chelator ethylene glycol tetra-acetic acid (EGTA) to remove extracellular calcium. We  
292 found that the Tg treatment rescued the decreased mTORC1 activity in BBOX1 KD cells, the

293 effect ameliorated by co-treatment with EGTA (**Supplementary Fig. S6D**). These data  
294 demonstrated that mTORC1 signaling could be activated by BBOX1-IP3R3 mediated calcium  
295 signaling. We next measured the extracellular acidification rate (ECAR) as an indicator of  
296 glycolysis in IP3R3- or BBOX1- depleted cells, and found that the glycolytic rate was decreased  
297 upon both IP3R3 and BBOX1 depletion (**Fig. 4J and K; Supplementary Fig. S6E**). Collectively,  
298 our data show that BBOX1 is also required for maintaining glycolysis through IP3R3-mediated  
299 calcium signaling in TNBC cells.

300 The mitochondrial respiration, mTORC1 activity and glycolysis deficiency induced by  
301 BBOX1 depletion subsequently corresponded with increased apoptosis measured by  
302 upregulated cleaved PARP, which was confirmed by flow cytometry analysis (**Fig. 4L;**  
303 **Supplementary Fig. S7A–S7D**). On the contrary, overexpression of BBOX1 but not the N2D  
304 mutant can protect TNBC cells from apoptosis as shown by cleaved PARP for the basal  
305 apoptotic level (**Supplementary Fig. S7E**). IP3R3 depletion in these TNBC cell lines  
306 recapitulated the apoptotic phenotype observed with BBOX1 knockdown (**Fig. 4M;**  
307 **Supplementary Fig. S7F–S7H**). Furthermore, we found that the G2/M cell cycle checkpoint  
308 was strongly enriched in the BBOX1 KD cells (**Supplementary Fig. S8A and S8B**), which was  
309 further confirmed by cell cycle analysis by flow cytometry with BBOX1 or IP3R3 depletion  
310 (**Supplementary Fig. S8C–S8F**). To validate IP3R3 as a critical downstream target of BBOX1  
311 for TNBC cell growth, we depleted IP3R3 in multiple TNBC cell lines and found decreased cell  
312 proliferation with MTS assay, 2-D colony formation assay and 3-D soft agar formation (**Fig. 4N;**  
313 **Supplementary Fig. S9A–S9D**). Notably, IP3R3 depletion in MCF-10A and HMLE did not  
314 cause significant cell growth defect (**Fig. 4N; Supplementary Fig. S9E and S9F**). To examine  
315 whether the phenotypic effects of BBOX1 on TNBC or breast epithelial cells are dependent on  
316 IP3R3, we overexpressed BBOX1 in multiple cell lines and observed increased S6K1 Thr389  
317 phosphorylation, OCR and cell proliferation, the effect ameliorated by concurrent IP3R3  
318 depletion (**Fig. 4O–R; Supplementary Fig. S9G–S9L**). It is worth noting that IP3R3 did not

319 associate with poor prognosis in TNBC/basal cancers (**Supplementary Fig. S9M**), which could  
320 be due to its post-transcriptional regulation by BBOX1. Collectively, our results suggest that  
321 IP3R3 is an important downstream functional mediator of BBOX1 effect on TNBC cell  
322 proliferation and survival. In addition, the effect of BBOX1 on cell proliferation could be multi-  
323 factorial, by affecting mTORC1/glycolysis as well as mitochondrial function.

324

### 325 **BBOX1 is a Novel Therapeutic Target in TNBC**

326 In order to examine the physiological relevance of targeting the BBOX1 signaling  
327 pathway in TNBC *in vivo*, firstly we generated cell lines with BBOX1 knockdown by using two  
328 independent shRNAs. We orthotopically injected these cells into the mammary fat pad of  
329 immunocompromised NOD scid gamma (NSG) mice and monitored the tumor growth over time.  
330 Consistent with the phenotype observed *in vitro*, BBOX1 depletion led to profound breast tumor  
331 growth defect *in vivo*, which correlated with decreased IP3R3 in tumors (**Fig. 5A–C;**  
332 **Supplementary Fig. S10A**). In addition, we also generated doxycycline-inducible BBOX1  
333 knockdown MDA-MB-468 cells with two independent shRNAs. In these cells, BBOX1 can be  
334 efficiently depleted upon doxycycline treatment, which led to efficient inhibition on 2-D colony  
335 formation as well as 3-D anchorage-independent growth (**Fig. 5D–G**). Then, one of these  
336 hairpin-infected tumor cells and the control cells were orthotopically injected into the mammary  
337 fat pad of NSG mice. Upon confirmation of tumor formation, we fed these mice with doxycycline  
338 to induce BBOX1 depletion. Whereas control cells (shCtrl) grew readily over time, BBOX1  
339 depletion significantly inhibited tumor growth and downstream IP3R3 level (**Fig. 5H–J;**  
340 **Supplementary Fig. S10B**). These data suggest that BBOX1 is important for maintaining  
341 TNBC tumor growth *in vivo*. It is important to note that tumor phenotype was more robust in  
342 Fig.5A compared to Fig.5H, which may be due to a longer time for doxycycline inducible  
343 shRNAs to take effect *in vivo* compared to non-inducible shRNAs.

344 As an orthogonal approach, we next investigated the pharmacological inhibition of  
345 BBOX1. To this end, we implemented Mildronate (40), a clinically approved drug, and two  
346 leading recently characterized BBOX1 inhibitor compounds: C-2124 (41) and AR692B (42).  
347 Mildronate and C-2124 are structural analogues of the BBOX1 enzymatic substrate GBB that  
348 abolish BBOX1 catalytic activity through competitive binding to its substrate pocket. AR692B, on  
349 the other hand, causes BBOX1 conformational changes (42). Firstly, we tested the effect of  
350 these inhibitors on disrupting the BBOX1-IP3R3 interaction. In fact, all these compounds  
351 inhibited the association between BBOX1 and IP3R3 endogenously or exogenously in multiple  
352 cell lines including MDA-468 and MDA-MB-231 in a dose-dependent manner (**Fig. 6A–D;**  
353 **Supplementary Fig. S11A– S11G**), which is consistent with the data we obtained with the  
354 BBOX1 catalytically dead mutant N2D. Next, we treated MDA-MB-468 cells with C-2124,  
355 Mildronate or AR692B and found that these compound treatments led to decreased IP3R3  
356 protein levels after extended period treatment (72 or 96 hours), whereas no effect observed  
357 after short-term treatment (24 hours) (**Supplementary Fig. S11H–S11J**). In addition, mTORC1  
358 signaling was significantly suppressed by these inhibitor treatments (**Fig. 6E and F;**  
359 **Supplementary Fig. S11K and S11L**). In line with the OCR decrease by BBOX1 depletion, C-  
360 2124 treatment also led to impaired OCR in MDA-MB-468 cells (**Supplementary Fig. S11M**).  
361 Cell viability was then assessed by treating a panel of breast cell lines with various doses of the  
362 inhibitors C-2124 or AR692B. We observed that the TNBC cell lines with high BBOX1  
363 expression (e.g. MDA-MB-468, HCC70) displayed higher sensitivity to the BBOX1 inhibitors  
364 compared with the non-TNBC cell lines with low BBOX1 expression (e.g. MCF-7, T47D, MCF-  
365 10A) (**Fig. 6G; Supplementary Fig. S12A**). Notably, this sensitivity was especially obvious in  
366 the range of low doses for these inhibitors. Furthermore, we conducted 3-D soft agar assay in  
367 these cells and found that these inhibitors suppressed anchorage-independent growth in TNBC  
368 cell lines including MDA-MB-468, HCC70, HCC3153 or MDA-MB-231 in a dose-dependent  
369 manner. Interestingly, these inhibitors did not affect MCF-7, T47D or HMLE cell growth (**Fig. 6H;**

370 **Supplementary Fig. S12B–S12D**), despite that intercellular carnitine level was profoundly  
371 decreased by the BBOX1 inhibitor treatment in these cells (**Supplementary Fig. S12E**).  
372 Therefore, BBOX1 protein level correlates to some extent with the efficacy of BBOX1 inhibitors  
373 in these cells. Additionally, 2-D colony formation assay showed that these inhibitors did not  
374 affect MCF-10A cell growth (**Supplementary Fig. S12F and S12G**). To further assess the  
375 specificity of the inhibitor, we treated MDA-MB-231 cells stably expressing WT BBOX1 or N2D  
376 mutant with various doses of C-2124 or vehicle. The cell viability assay showed that MDA-MB-  
377 231 expressing the WT BBOX1 presented higher sensitivity compared with MDA-MB-231 N2D  
378 cells (**Fig. 6I**). As a proof of principle, we examined the efficacy of the BBOX1 inhibitor *in vivo*.  
379 We treated the MDA-MD-468 xenograft breast tumor bearing NSG mice with Mildronate and  
380 found that it efficiently suppressed the tumor growth *in vivo* (**Fig. 6J–6L**). Importantly, these  
381 treatments did not affect the mice body weight (**Fig. 6M**), suggesting that the drug does not  
382 carry significant toxicity in mice and the effect of these BBOX1 inhibitors on TNBC is specific.

383

## 384 **DISCUSSION**

385 In this study, we have identified BBOX1 as a potential new target in TNBC by modulating  
386 IP3R3 protein stability, calcium homeostasis, cellular bioenergetics and cancer cell fate. In  
387 summary, BBOX1 protects IP3R3 from FBXL2 mediated proteasomal degradation and  
388 maintains IP3R3 mediated constitutive calcium flux from ER that is essential for sustaining  
389 mitochondrial function and activating mTORC1-mediated glycolysis. Both metabolic pathways  
390 are critical for providing the demand of energy and biochemical intermediates for cancer cell  
391 proliferation and tumorigenesis. On the other hand, either *BBOX1* genetic depletion or the  
392 pharmacological abrogation of BBOX1-IP3R3 interaction blocks this oncogenic calcium  
393 signaling, impairing cellular metabolism and eventually causing cancer cell death (**Fig. 6N**).

394 TNBC is a heterogeneous and lethal disease among women with limited therapeutic  
395 options (43) and discovery of new targeted therapies is required. We performed the initial  
396 screening from a library targeting the whole family of known 2-OG dependent enzymes because:  
397 1) they play a role as oxygen sensors in the mammalian cell to regulate a broad spectrum of  
398 cellular processes. For instance, the proline hydroxylase EglNs governing HIF $\alpha$  protein stability  
399 regulation under different oxygenic scenarios (normoxia/hypoxia), therefore contribute to  
400 malignancies in cancer (44); 2) emerging literature uncovers their critical roles in cancer  
401 progression or suppression, while an unbiased systematic approach to investigate their role in  
402 cancer is lacking ; 3) there are actionable therapeutic drugs have been or can be developed to  
403 target some of these enzymes (45). In this paper, we show a novel role of BBOX1 in breast  
404 cancer tumorigenesis, independent of its canonical function in carnitine synthesis. By TAP-TAG  
405 purification followed by mass spectrometry, we identify IP3R3 as an important binding partner  
406 and downstream factor of BBOX1. Our finding indicates the novel role of the 2-OG dependent  
407 enzymes regulating numerous non-canonical substrates or binding partners, which deserve  
408 further investigation. One limitation of our study is that we have not demonstrated whether  
409 BBOX1 can catalyze hydroxylation reaction beyond GBB and use large molecules such as  
410 proteins as substrates. We speculate that it is of high possibility since IP3R3 binding with  
411 BBOX1 largely depends on its catalytic activity, which warrants further investigation.

412 Calcium signaling plays vital roles in various cellular processes (46) and has been  
413 largely reported to associate with cancer progression (47,48). Calcium dependent signaling  
414 pathways are frequently dysregulated or altered in cancer cells to meet the demand of cell  
415 proliferation, invasion, and metastasis (47). The IP3 receptors are principal Ca<sup>2+</sup> channels  
416 located on the ER membrane and essential for the control of intracellular Ca<sup>2+</sup> levels (49). There  
417 are three family IP3R members (IP3R1, IP3R2, and IP3R3) while IP3R3 is emerging as the  
418 isoform that is particularly important in the pathogenesis of human diseases (50). Increases of  
419 IP3R3 expression occur in a variety of malignancies, such as colorectal cancer, glioblastoma,

420 breast cancer and kidney cancer (23-26). Previous studies reported that IP3R3 mediated  
421 calcium signaling positively regulates migration (31) and cell growth under certain conditions (51)  
422 in the MCF-7 breast cancer cell line. Our study confirms the universal role of calcium and  
423 highlights that TNBC cells are particularly addictive to the IP3R3-Ca<sup>2+</sup> signaling axis. We identify  
424 BBOX1 as an upstream regulator of this IP3R3-Ca<sup>2+</sup> signaling controlling various critical  
425 metabolic pathways (e.g. TCA cycle, glycolysis, and nucleotide metabolism). Besides, BBOX1  
426 depletion-induced cell cycle change may largely due to its effect on calcium signaling, since it is  
427 well documented that calcium is a critical regulator of cell cycle progression (47). Therefore,  
428 targeting the aberrant calcium signaling may be beneficial for certain cancers such as TNBC  
429 (52).

430 In this study, we incorporated several BBOX1 inhibitors to target TNBC cell growth and  
431 tumorigenesis *in vitro* and *in vivo*. As a proof of principle of our finding, these inhibitors showed  
432 some efficacy by blocking the BBOX1-IP3R3 interaction, suppressing the oncogenic calcium  
433 signaling, altering cell metabolism and killing TNBC cells. Meldonium (trade name Mildronate),  
434 developed in 1970 by Latvia Institute of Organic Synthesis, is widely used as an anti-ischemia  
435 drug in Eastern Europe, and was shown to be safe and well-tolerated (53,54). According to the  
436 previous literature, the Km of Meldonium towards rat BBOX1 was 37  $\mu$ M (55), which explains  
437 why we need higher dosage to be used in human cancer cell lines. However, it is important to  
438 point out that at the dosage used, these inhibitors did not appear to affect normal breast  
439 epithelial cell proliferation (**Fig. 6H; Fig. S12C and S12D**). These inhibitors appear to be non-  
440 toxic in multiple models used including dogs and rats (56). For example, 800 mg/kg was used in  
441 the rat model with no obvious toxicity (57). However, it is important to acknowledge that  
442 Meldonium might likely inhibit OCTN2 (58), In addition, our current model is not enough to  
443 support the finding since we have not examined the drug in more clinically relevant models such  
444 as the patient-derived xenografts (PDXs). Novel BBOX inhibitors have been developed and

445 show better selectivity and efficacy to some extent (41,42), as we also observed in our study. In  
446 summary, our study provides the evidence that BBOX1 is a new therapeutic target in TNBC,  
447 which hopefully will motivate the development of specific and potent BBOX1 inhibitors in this  
448 lethal disease.

449 **METHODS**

450 **Cell Culture.** MDA-MB-231, MDA-MB-436, *Hs578T*, MCF-7, BT474, and 293T cells were  
451 cultured in Dulbecco's Modified Eagle's Medium (DMEM) (Gibco 11965118) supplemented with  
452 10% fetal bovine serum (FBS) and 1% penicillin-streptomycin (Pen Strep). T47D, HCC3153,  
453 HCC1187, HCC70 and MDA-MB-468 cells were cultured in 10% FBS, 1% Pen Strep RPMI  
454 1640 (Gibco 11875093). Normal breast epithelial cells HMLE and MCF-10A were cultured in  
455 MEGM (Lonza CC-3151) containing SingleQuotes Supplements (Lonza CC-4136). SUM149 cells  
456 were cultured in HuMEC Ready Medium (Gibco 12752-010). HCC3153 were obtained from the  
457 cell repository of the Hamon Center for Therapeutic Oncology Research, UT Southwestern  
458 Medical Center. HMLE was obtained from Dr. Wenjun Guo. All other cell lines were obtained  
459 from ATCC. Cells were used for experiments within 10-20 passages from thawing. All cells were  
460 authenticated via short tandem repeat testing. Mycoplasma detection was routinely performed  
461 to ensure cells were not infected with mycoplasma by using MycoAlert Detection kit (Lonza,  
462 LT07-218).

463  
464 **Antibodies and Reagents.** Rabbit anti BBOX1 (ab171959), goat anti FBXL2 (ab17018) were  
465 from Abcam. Mouse anti IP3R3 (610312) was from BD Biosciences. Rabbit anti TMLHE (16621-  
466 1-AP), rabbit anti-ALKBH4 (19882-1-AP) were from Proteintech. Rabbit anti HIF-1 $\alpha$  (3716),  
467 rabbit anti PTEN (9559S), rabbit anti HA tag (3724), rabbit anti Flag-tag (14793), rabbit anti V5-  
468 tag (13202), mouse anti His-tag (2366), rabbit anti cleaved-caspase 3 (9664), rabbit anti PARP  
469 (9532), mouse anti  $\alpha$ -Tubulin (3873) were from Cell Signaling Technology. Mouse anti Ub  
470 (8017), mouse anti  $\beta$ -actin (sc-47778) were from Santa Cruz. Mouse anti vinculin (V9131) was  
471 from Sigma-Aldrich. Antibodies used for IHC staining were rabbit anti IP3R3 (Bethyl  
472 Laboratories, 50-157-2451), mouse anti BBOX1 (Sigma-Aldrich, WH0008424M1). Mildronate  
473 (S4130) was from Selleckchem. C-2124 was kindly provided by Latvian Institute of Organic

474 Synthesis (41). AR692B was synthesized by WuxiAPP Tech following the procedure described  
475 previously (42). MTS reagents (ab197010) was from Abcam. Doxycycline (D9891), MLN-4924  
476 (5054770001) were from Sigma-Aldrich, DMOG (D1070-1g) was from Frontier Scientific,  
477 MG132 (IZL-3175-v) was from Peptide International.

478

#### 479 **2-D Cell Proliferation Assay and 3-D Soft Agar Growth Assay.**

480 For MTS assay, Cells were seeded in 96-well plates (1000~2000 cells/well) in appropriate  
481 growth medium, the rest of the steps were performed as previously described (59). The colony  
482 formation assay and 3-D soft agar assay were performed as previously described (60). For  
483 colony formation assay, cells were seeded in duplicate in 6-well plates ( $1 \times 10^5$  cells/well). For  
484 inhibitor treatments, BBOX1 inhibitors were added the following day after seeding the cells and  
485 was renewed every day.

486

487 **Immunoblotting and Immunoprecipitation.** EBC buffer (50mM Tris-HCl pH8.0, 120 mM NaCl,  
488 0.5% NP40, 0.1 mM EDTA and 10% glycerol) supplemented with complete protease inhibitor  
489 and phosphoSTOP tablets (Roche Applied Bioscience) was used to harvest whole cell lysates  
490 at 4°C. Cell lysate concentration was measured by Protein assay dye (BioRad). Equal amount  
491 of cell lysates was resolved by SDS-PAGE. For immunoprecipitation, whole-cell lysates were  
492 prepared in EBC buffer supplemented with protease inhibitor and phosphatase inhibitor. The  
493 lysates were clarified by centrifugation and then incubated with primary antibodies or FLAG/HA  
494 antibody-conjugated beads (FLAG M2 beads, Sigma; HA beads, Roche Applied Bioscience)  
495 overnight at 4°C. For primary antibody incubation, cell lysates were incubated further with  
496 protein G sepharose beads (Roche Applied Bioscience) for 2 hours at 4°C. The bound  
497 complexes were washed with EBC buffer for 3x times and were eluted by boiling in SDS loading  
498 buffer. Bound proteins were resolved in SDS-PAGE followed by immunoblotting analysis.

499

500 **RNA-Seq Analysis.** Total RNA from triplicates was extracted from MDA-MB-468 cells infected  
501 with control or BBOX1 shRNAs by using RNeasy kit with on column DNase digestion (Qiagen).  
502 Library preparation and sequencing were performed by BGI as paired-end 100bp reads followed  
503 by the same analysis pipeline as described previously (59). Gene set enrichment analysis  
504 (GSEA) was performed by using the GSEA software and Hallmark signatures. RNA-seq data  
505 are deposited to GEO under accession number GSE152317.

506

507 **OCR and ECAR Measurement.** The OCR and ECAR were measured by an XFe24  
508 extracellular flux analyzer (Agilent Technologies), according to the manufacturer's instructions.  
509 Briefly, a total of  $1 \times 10^5$  cells were seeded into XF24 cell culture microplate coated with CellTak  
510 (Corning) before the assay. Detailed experimental procedures were described in the  
511 supplementary method.

512

513 **Survival Analysis.** The effects of *BBOX1* gene and IP3 receptor family genes (*ITPR1*, 2 and 3)  
514 on the survival of patients with breast cancer were performed using the Kaplan Meier Plotter  
515 online survival analysis tool (<https://kmplot.com/analysis/>). To obtain sufficient patient samples,  
516 the relapse-free survival (DFS) mode was used to conduct all the analyses.

517

518 **Orthotopic Tumor Xenograft.** Six-week old female NOD SCID Gamma mice (NSG, Jackson  
519 lab) were used for xenograft studies. Approximately  $5 \times 10^5$  viable MDA-MB-468 cells expressing  
520 control/BBOX1 shRNAs or Teton BBOX1 shRNA, or  $1 \times 10^6$  viable MDA-MB-468 parental cells  
521 were resuspended in 100  $\mu$ l matrigel (Corning, 354234) and injected orthotopically into the  
522 mammary fat pad of each mouse. For inducible BBOX1 shRNA, after cell injection and following  
523 two consecutive weeks of tumor monitoring to make sure tumor was successfully implanted,  
524 mice were fed Purina rodent chow with doxycycline (Research Diets Inc., #5001). For BBOX1  
525 inhibitors treatment, when tumors reached the volume of approximately 60 mm<sup>3</sup>, mice were

526 divided in two groups by randomization, 400 mg/kg body weight of Mildronate or the vehicle  
527 saline was given through Intraperitoneal injection. Tumor size was measured using an electronic  
528 clipper. Tumor volumes were calculated with the formula:  $\text{volume} = (L \times W^2)/2$ , where L is the  
529 tumor length and W is the tumor width measured in millimeters. All animal experiments were in  
530 compliance with National Institutes of Health guidelines and were approved by the University of  
531 North Carolina at Chapel Hill Animal Care and Use Committee.

532

533 **Statistical Analysis.** All statistical analysis was conducted using Prism 8.0 (GraphPad  
534 Software). All graphs depict mean  $\pm$  SEM unless otherwise indicated. Statistical significances  
535 are denoted as n.s. (not significant;  $P > 0.05$ ), \* $P < 0.05$ , \*\* $P < 0.01$ , \*\*\* $P < 0.001$ , \*\*\*\* $P < 0.0001$ .  
536 The numbers of experiments are noted in figure legends. To assess the statistical significance  
537 of a difference between two conditions, we used unpaired two-tail student's *t*-test. For  
538 experiments comparing more than two conditions, differences were tested by a one-way  
539 ANOVA followed by Dunnett's or Tukey's multiple comparison tests.

540

541 **Acknowledgments**

542 We thank all members of the Zhang, Perou, and Yang laboratories for helpful discussions and  
543 suggestions. We thank Dr. Ralph DeBerardinis and Children's Research Institute (CRI)'s  
544 Metabolomics Facility at UTSW for their helps. We thank Shafi Kuchay and Michele Pagano for  
545 providing the IP3R3 mutant plasmids. We thank Osvalds Pugovics for the help of BBOX1  
546 inhibitors. We thank Yongjuan Xia, Stephanie Cohen and Nana Nikolaishvili-Feinberg in the  
547 UNC Translational Pathology Laboratory for the IHC staining and data analysis. We thank  
548 Charlene Santos and colleagues in the UNC Animal Studies Core for the help of animal  
549 studies. This research is supported by Cancer Prevention and Research Institute of Texas  
550 (CPRIT, RR190058 to Q.Z). C.M.P is supported by NCI Breast SPORE program (P50-  
551 CA58223), R01-CA148761 and the Breast Cancer Research Foundation. Q.Z is also supported  
552 by the National Cancer Institute (R01CA211732) and American Cancer Society (RSG TBE-  
553 132187). This research is based in part upon work conducted using the UNC Proteomics Core  
554 Facility, which is supported in part by P30 CA016086 Cancer Center Core Support Grant to the  
555 UNC Lineberger Comprehensive Cancer Center.

556

557 **Author contributions**

558 C. L. and Q. Z. conceived, performed and interpreted experiments. C. L. and Q. Z. wrote the  
559 paper with critical comments from all authors. C. F. performed the patient data analysis. J. L.  
560 and J. W. L. performed the metabolomics study. J. M. S. and T. S. P. provided the RNA-seq  
561 bioinformatics analysis. Y. Z. performed the calcium measurement. L. E. H. performed mass  
562 spectrometry analysis. V. G. A. and E. L. contributed to inhibitors synthesis. C. M. P., H. Y., Y.  
563 P., G. Z., and L. H. helped to provide critical advice and reagents for the paper. M. T. and J. Z.  
564 contributed to acquisition of data during revision.

565

566 **Competing interests**

567 C.M.P is an equity stock holder and consultant of BioClassifier LLC; C.M.P is also listed an  
568 inventor on patent applications on the Breast PAM50 Subtyping assay.

569

## 570 REFERENCES

- 571
- 572 1. Anders CK, Carey LA. Biology, metastatic patterns, and treatment of patients with triple-  
573 negative breast cancer. *Clin Breast Cancer* **2009**;9 Suppl 2:S73-81 doi  
574 10.3816/CBC.2009.s.008.
  - 575 2. Metzger O, Tutt A, de Azambuja E, Saini KS, Viale G, Loi S, *et al.* Dissecting the  
576 Heterogeneity of Triple-Negative Breast Cancer. *J Clin Oncol* **2012**;30(15):1879-87 doi  
577 10.1200/Jco.2011.38.2010.
  - 578 3. Wahba HA, El-Hadaad HA. Current approaches in treatment of triple-negative breast  
579 cancer. *Cancer Biol Med* **2015**;12(2):106-16 doi 10.7497/j.issn.2095-3941.2015.0030.
  - 580 4. Losman JA, Kaelin WG, Jr. What a difference a hydroxyl makes: mutant IDH, (R)-2-  
581 hydroxyglutarate, and cancer. *Genes & development* **2013**;27(8):836-52 doi  
582 10.1101/gad.217406.113.
  - 583 5. Zheng X, Zhai B, Koivunen P, Shin SJ, Lu G, Liu J, *et al.* Prolyl hydroxylation by EglN2  
584 destabilizes FOXO3a by blocking its interaction with the USP9x deubiquitinase. *Genes &*  
585 *development* **2014**;28(13):1429-44 doi 10.1101/gad.242131.114.
  - 586 6. Kaelin WG, Jr., Ratcliffe PJ. Oxygen sensing by metazoans: the central role of the HIF  
587 hydroxylase pathway. *Molecular cell* **2008**;30(4):393-402 doi  
588 10.1016/j.molcel.2008.04.009.
  - 589 7. Cloos PA, Christensen J, Agger K, Helin K. Erasing the methyl mark: histone  
590 demethylases at the center of cellular differentiation and disease. *Genes & development*  
591 **2008**;22(9):1115-40 doi 10.1101/gad.1652908.
  - 592 8. Varier RA, Timmers HT. Histone lysine methylation and demethylation pathways in  
593 cancer. *Biochimica et biophysica acta* **2011**;1815(1):75-89 doi  
594 10.1016/j.bbcan.2010.10.002.
  - 595 9. Takada M, Zhuang M, Inuzuka H, Zhang J, Zurlo G, Zhang JF, *et al.* EglN2 contributes  
596 to triple negative breast tumorigenesis by functioning as a substrate for the FBW7 tumor  
597 suppressor. *Oncotarget* **2017**;8(4):6787-95 doi 10.18632/oncotarget.14290.
  - 598 10. Zurlo G, Liu XJ, Takada M, Fan C, Simon JM, Ptacek TS, *et al.* Prolyl hydroxylase  
599 substrate adenylosuccinate lyase is an oncogenic driver in triple negative breast cancer.  
600 *Nature Communications* **2019**;10:5177 doi 10.1038/s41467-019-13168-4.
  - 601 11. Paul HS, Sekas G, Adibi SA. Carnitine biosynthesis in hepatic peroxisomes.  
602 Demonstration of gamma-butyrobetaine hydroxylase activity. *Eur J Biochem*  
603 **1992**;203(3):599-605 doi 10.1111/j.1432-1033.1992.tb16589.x.
  - 604 12. Kim JH, Sharma A, Dhar SS, Lee SH, Gu B, Chan CH, *et al.* UTX and MLL4  
605 coordinately regulate transcriptional programs for cell proliferation and invasiveness in  
606 breast cancer cells. *Cancer research* **2014**;74(6):1705-17 doi 10.1158/0008-5472.CAN-  
607 13-1896.
  - 608 13. Lee YF, Miller LD, Chan XB, Black MA, Pang B, Ong CW, *et al.* JMJD6 is a driver of  
609 cellular proliferation and motility and a marker of poor prognosis in breast cancer. *Breast*  
610 *cancer research : BCR* **2012**;14(3):R85 doi 10.1186/bcr3200.
  - 611 14. Cancer Genome Atlas N. Comprehensive molecular portraits of human breast tumours.  
612 *Nature* **2012**;490(7418):61-70 doi 10.1038/nature11412.

- 613 15. Curtis C, Shah SP, Chin SF, Turashvili G, Rueda OM, Dunning MJ, *et al.* The genomic  
614 and transcriptomic architecture of 2,000 breast tumours reveals novel subgroups. *Nature*  
615 **2012**;486(7403):346-52 doi 10.1038/nature10983.
- 616 16. Prat A, Parker JS, Karginova O, Fan C, Livasy C, Herschkowitz JI, *et al.* Phenotypic and  
617 molecular characterization of the claudin-low intrinsic subtype of breast cancer. *Breast*  
618 *cancer research : BCR* **2010**;12(5):R68 doi 10.1186/bcr2635.
- 619 17. Badve S, Dabbs DJ, Schnitt SJ, Baehner FL, Decker T, Eusebi V, *et al.* Basal-like and  
620 triple-negative breast cancers: a critical review with an emphasis on the implications for  
621 pathologists and oncologists. *Mod Pathol* **2011**;24(2):157-67 doi  
622 10.1038/modpathol.2010.200.
- 623 18. Leung IK, Krojer TJ, Kochan GT, Henry L, von Delft F, Claridge TD, *et al.* Structural and  
624 mechanistic studies on gamma-butyrobetaine hydroxylase. *Chem Biol*  
625 **2010**;17(12):1316-24 doi 10.1016/j.chembiol.2010.09.016.
- 626 19. Vaz FM, van Gool S, Ofman R, Ijlst L, Wanders RJ. Carnitine biosynthesis: identification  
627 of the cDNA encoding human gamma-butyrobetaine hydroxylase. *Biochem Biophys Res*  
628 *Commun* **1998**;250(2):506-10 doi 10.1006/bbrc.1998.9343.
- 629 20. Bremer J. Carnitine--metabolism and functions. *Physiol Rev* **1983**;63(4):1420-80 doi  
630 10.1152/physrev.1983.63.4.1420.
- 631 21. Chong J, Wishart DS, Xia J. Using MetaboAnalyst 4.0 for Comprehensive and  
632 Integrative Metabolomics Data Analysis. *Curr Protoc Bioinformatics* **2019**;68(1):e86 doi  
633 10.1002/cpbi.86.
- 634 22. Rizzuto R, Marchi S, Bonora M, Aguiari P, Bononi A, De Stefani D, *et al.* Ca<sup>2+</sup> transfer  
635 from the ER to mitochondria: When, how and why. *Biochimica Et Biophysica Acta-*  
636 *Bioenergetics* **2009**;1787(11):1342-51 doi 10.1016/j.bbabi.2009.03.015.
- 637 23. Shibao K, Fiedler MJ, Nagata J, Minagawa N, Hirata K, Nakayama Y, *et al.* The type III  
638 inositol 1,4,5-trisphosphate receptor is associated with aggressiveness of colorectal  
639 carcinoma. *Cell Calcium* **2010**;48(6):315-23 doi DOI 10.1016/j.ceca.2010.09.005.
- 640 24. Kang SS, Han KS, Ku BM, Lee YK, Hong J, Shin HY, *et al.* Caffeine-Mediated Inhibition  
641 of Calcium Release Channel Inositol 1,4,5-Trisphosphate Receptor Subtype 3 Blocks  
642 Glioblastoma Invasion and Extends Survival. *Cancer Res* **2010**;70(3):1173-83 doi  
643 10.1158/0008-5472.Can-09-2886.
- 644 25. Mound A, Rodat-Despoix L, Bougarn S, Ouadid-Ahidouch H, Matifat F. Molecular  
645 interaction and functional coupling between type 3 inositol 1,4,5-trisphosphate receptor  
646 and BKCa channel stimulate breast cancer cell proliferation. *European Journal of*  
647 *Cancer* **2013**;49(17):3738-51 doi 10.1016/j.ejca.2013.07.013.
- 648 26. Rezuchova I, Hudecova S, Soltysova A, Matuskova M, Durinikova E, Chovancova B, *et*  
649 *al.* Type 3 inositol 1,4,5-trisphosphate receptor has antiapoptotic and proliferative role in  
650 cancer cells. *Cell Death & Disease* **2019**;10:186 doi 10.1038/s41419-019-1433-4.
- 651 27. Kuchay S, Giorgi C, Simoneschi D, Pagan J, Missiroli S, Saraf A, *et al.* PTEN  
652 counteracts FBXL2 to promote IP3R3- and Ca(2+)-mediated apoptosis limiting tumour  
653 growth. *Nature* **2017**;546(7659):554-8 doi 10.1038/nature22965.
- 654 28. Emanuele MJ, Elia AE, Xu Q, Thoma CR, Izhar L, Leng Y, *et al.* Global identification of  
655 modular cullin-RING ligase substrates. *Cell* **2011**;147(2):459-74 doi  
656 10.1016/j.cell.2011.09.019.
- 657 29. Detre S, Saclani Jotti G, Dowsett M. A "quickscore" method for immunohistochemical  
658 semiquantitation: validation for oestrogen receptor in breast carcinomas. *J Clin Pathol*  
659 **1995**;48(9):876-8 doi 10.1136/jcp.48.9.876.
- 660 30. Cardenas C, Miller RA, Smith I, Bui T, Molgo J, Muller M, *et al.* Essential regulation of  
661 cell bioenergetics by constitutive InsP3 receptor Ca<sup>2+</sup> transfer to mitochondria. *Cell*  
662 **2010**;142(2):270-83 doi 10.1016/j.cell.2010.06.007.

- 663 31. Mound A, Vautrin-Glabik A, Foulon A, Botia B, Hague F, Parys JB, *et al.* Downregulation  
664 of type 3 inositol (1,4,5)-trisphosphate receptor decreases breast cancer cell migration  
665 through an oscillatory Ca<sup>2+</sup> signal. *Oncotarget* **2017**;8(42):72324-41 doi  
666 10.18632/oncotarget.20327.
- 667 32. Liberti MV, Locasale JW. The Warburg Effect: How Does it Benefit Cancer Cells? (vol 41,  
668 pg 211, 2016). *Trends Biochem Sci* **2016**;41(3):287- doi 10.1016/j.tibs.2016.01.004.
- 669 33. Brown KK, Spinelli JB, Asara JM, Toker A. Adaptive Reprogramming of De Novo  
670 Pyrimidine Synthesis Is a Metabolic Vulnerability in Triple-Negative Breast Cancer (vol 7,  
671 pg 391, 2017). *Cancer Discov* **2017**;7(7):782- doi 10.1158/2159-8290.Cd-17-0565.
- 672 34. Laplante M, Sabatini DM. mTOR signaling in growth control and disease. *Cell*  
673 **2012**;149(2):274-93 doi 10.1016/j.cell.2012.03.017.
- 674 35. Ben-Sahra I, Manning BD. mTORC1 signaling and the metabolic control of cell growth.  
675 *Curr Opin Cell Biol* **2017**;45:72-82 doi 10.1016/j.ceb.2017.02.012.
- 676 36. Gulati P, Gaspers LD, Dann SG, Joaquin M, Nobukuni T, Natt F, *et al.* Amino acids  
677 activate mTOR complex 1 via Ca<sup>2+</sup>/CaM signaling to hVps34. *Cell Metab*  
678 **2008**;7(5):456-65 doi 10.1016/j.cmet.2008.03.002.
- 679 37. Mercan F, Lee H, Kolli S, Bennett AM. Novel role for SHP-2 in nutrient-responsive  
680 control of S6 kinase 1 signaling. *Mol Cell Biol* **2013**;33(2):293-306 doi  
681 10.1128/MCB.01285-12.
- 682 38. Li RJ, Xu J, Fu C, Zhang J, Zheng YG, Jia H, *et al.* Regulation of mTORC1 by lysosomal  
683 calcium and calmodulin. *Elife* **2016**;5 doi 10.7554/eLife.19360.
- 684 39. Thastrup O, Cullen PJ, Drobak BK, Hanley MR, Dawson AP. Thapsigargin, a tumor  
685 promoter, discharges intracellular Ca<sup>2+</sup> stores by specific inhibition of the endoplasmic  
686 reticulum Ca<sup>2+</sup>(+)-ATPase. *Proc Natl Acad Sci U S A* **1990**;87(7):2466-70 doi  
687 10.1073/pnas.87.7.2466.
- 688 40. Simkhovich BZ, Shutenko ZV, Meirena DV, Khagi KB, Mezapuke RJ, Molodchina TN, *et*  
689 *al.* 3-(2,2,2-Trimethylhydrazinium)propionate (THP)--a novel gamma-butyrobetaine  
690 hydroxylase inhibitor with cardioprotective properties. *Biochem Pharmacol*  
691 **1988**;37(2):195-202 doi 10.1016/0006-2952(88)90717-4.
- 692 41. Tars K, Leitans J, Kazaks A, Zelencova D, Liepinsh E, Kuka J, *et al.* Targeting carnitine  
693 biosynthesis: discovery of new inhibitors against gamma-butyrobetaine hydroxylase.  
694 *Journal of medicinal chemistry* **2014**;57(6):2213-36 doi 10.1021/jm401603e.
- 695 42. Rydzik AM, Chowdhury R, Kochan GT, Williams ST, McDonough MA, Kawamura A, *et*  
696 *al.* Modulating carnitine levels by targeting its biosynthesis pathway - selective inhibition  
697 of gamma-butyrobetaine hydroxylase. *Chem Sci* **2014**;5(5):1765-71 doi  
698 10.1039/C4SC00020J.
- 699 43. Bianchini G, Balko JM, Mayer IA, Sanders ME, Gianni L. Triple-negative breast cancer:  
700 challenges and opportunities of a heterogeneous disease. *Nat Rev Clin Oncol*  
701 **2016**;13(11):674-90 doi 10.1038/nrclinonc.2016.66.
- 702 44. Ivan M, Kondo K, Yang H, Kim W, Valiando J, Ohh M, *et al.* HIF $\alpha$  targeted for VHL-  
703 mediated destruction by proline hydroxylation: implications for O<sub>2</sub> sensing. *Science*  
704 **2001**;292(5516):464-8 doi 10.1126/science.1059817.
- 705 45. Chan MC, Holt-Martyn JP, Schofield CJ, Ratcliffe PJ. Pharmacological targeting of the  
706 HIF hydroxylases--A new field in medicine development. *Mol Aspects Med* **2016**;47-  
707 48:54-75 doi 10.1016/j.mam.2016.01.001.
- 708 46. Clapham DE. Calcium signaling. *Cell* **2007**;131(6):1047-58 doi  
709 10.1016/j.cell.2007.11.028.
- 710 47. Roderick HL, Cook SJ. Ca<sup>2+</sup> signalling checkpoints in cancer: remodelling Ca<sup>2+</sup> for  
711 cancer cell proliferation and survival. *Nat Rev Cancer* **2008**;8(5):361-75 doi  
712 10.1038/nrc2374.

- 713 48. Monteith GR, Prevarskaya N, Roberts-Thomson SJ. The calcium-cancer signalling  
714 nexus. *Nat Rev Cancer* **2017**;17(6):367-80 doi 10.1038/nrc.2017.18.
- 715 49. Foskett JK, White C, Cheung KH, Mak DO. Inositol trisphosphate receptor Ca<sup>2+</sup> release  
716 channels. *Physiol Rev* **2007**;87(2):593-658 doi 10.1152/physrev.00035.2006.
- 717 50. Mangla A, Guerra MT, Nathanson MH. Type 3 inositol 1,4,5-trisphosphate receptor: A  
718 calcium channel for all seasons. *Cell Calcium* **2020**;85:102132 doi  
719 10.1016/j.ceca.2019.102132.
- 720 51. Szatkowski C, Parys JB, Ouadid-Ahidouch H, Matifat F. Inositol 1,4,5-trisphosphate-  
721 induced Ca<sup>2+</sup> signalling is involved in estradiol-induced breast cancer epithelial cell  
722 growth. *Molecular Cancer* **2010**;9:156 doi 10.1186/1476-4598-9-156.
- 723 52. Cui C, Merritt R, Fu L, Pan Z. Targeting calcium signaling in cancer therapy. *Acta Pharm*  
724 *Sin B* **2017**;7(1):3-17 doi 10.1016/j.apsb.2016.11.001.
- 725 53. Zhu Y, Zhang GY, Zhao J, Li DS, Yan XD, Liu JF, *et al.* Efficacy and Safety of  
726 Mildronate for Acute Ischemic Stroke: A Randomized, Double-Blind, Active-Controlled  
727 Phase II Multicenter Trial. *Clin Drug Invest* **2013**;33(10):755-60 doi 10.1007/s40261-013-  
728 0121-x.
- 729 54. Dzerve V, Group MIS. A dose-dependent improvement in exercise tolerance in patients  
730 with stable angina treated with mildronate: a clinical trial "MILSS I". *Medicina (Kaunas)*  
731 **2011**;47(10):544-51.
- 732 55. Spaniol M, Brooks H, Auer L, Zimmermann A, Solioz M, Stieger B, *et al.* Development  
733 and characterization of an animal model of carnitine deficiency. *Eur J Biochem*  
734 **2001**;268(6):1876-87.
- 735 56. Liepinsh E, Dambrova M. The unusual pharmacokinetics of meldonium: Implications for  
736 doping. *Pharmacol Res* **2016**;111:100 doi 10.1016/j.phrs.2016.05.029.
- 737 57. Degrace P, Demizieux L, Du ZY, Gresti J, Caverot L, Djaouti L, *et al.* Regulation of lipid  
738 flux between liver and adipose tissue during transient hepatic steatosis in carnitine-  
739 depleted rats. *The Journal of biological chemistry* **2007**;282(29):20816-26 doi  
740 10.1074/jbc.M611391200.
- 741 58. Fink MA, Paland H, Herzog S, Grube M, Vogelgesang S, Weitmann K, *et al.* L-Carnitine-  
742 Mediated Tumor Cell Protection and Poor Patient Survival Associated with OCTN2  
743 Overexpression in Glioblastoma Multiforme. *Clinical cancer research : an official journal*  
744 *of the American Association for Cancer Research* **2019**;25(9):2874-86 doi  
745 10.1158/1078-0432.CCR-18-2380.
- 746 59. Liu XJ, Simon JM, Xie HB, Hu LX, Wang J, Zurlo G, *et al.* Genome-wide Screening  
747 Identifies SFMBT1 as an Oncogenic Driver in Cancer with VHL Loss. *Molecular Cell*  
748 **2020**;77(6):1294-306 doi 10.1016/j.molcel.2020.01.009.
- 749 60. Hu LX, Xie HB, Liu XJ, Potjewyd F, James LI, Wilkerson EM, *et al.* TBK1 Is a Synthetic  
750 Lethal Target in Cancer with VHL Loss. *Cancer Discov* **2020**;10(3):460-75 doi  
751 10.1158/2159-8290.Cd-19-0837.
- 752

753 **FIGURE LEGENDS**

754 **Figure 1. BBOX1 is required for TNBC cell growth.**

755 **A**, Overlay of MTS assay and soft agar results for the screening. GAPDH was used as a  
756 positive control for the siRNA library screening.  
757 **B**, Dot plot shows the genes scored both in the MTS assay and in the soft agar screening.  $q <$   
758  $0.001$  (MTS assay) and  $q < 0.000001$  (soft agar) were used as cutoff.  
759 **C**, Lists of genes identified significant growth changing in MTS assay and soft agar of MDA-MB-  
760 231.  
761 **D**, Soft agar colony growth of TNBC cells (MDA-MB-231, 436, 468) transfected with non-  
762 targeting (NT) siRNA control or two individual BBOX1 siRNAs.  
763 **E**, Quantification of the soft agar colony number related to D. Error bars represent SEM, two-  
764 tailed Student's t-test, \* $P < 0.05$ , \*\* $P < 0.01$ .  
765 **F**, Immunoblot of endogenous BBOX1 and TMLHE protein levels in a panel of normal breast  
766 epithelial cell lines and breast cancer cell lines. s.e., short exposure time, l.e., long exposure  
767 time.  
768 **G**, BBOX1 mRNA expression across different subtypes of breast cancer in TCGA, METABRIC  
769 and UNC337 datasets. Sample numbers were shown above each subtype.  
770 **H**, Kaplan-Meier plots of survival data for breast cancer patients with intrinsic subtypes stratified  
771 by *BBOX1* mRNA expression levels. Patient numbers were shown.

772  
773

774 **Figure 2. BBOX1 promotes TNBC cell growth in an enzymatically dependent fashion.**

775 **A-C**, Immunoblot analysis (A), 2-D colony formation assay (B) and representative soft agar  
776 images (C) of indicated BBOX1 depleted breast cancer cells or normal epithelial cells. BBOX1  
777 expression level of cells was indicated according to Fig. 1F.  
778 **D-E**, Immunoblot analysis (D) and MTS cell proliferation (E) of MDA-MB-231 stable cell lines  
779 expressing control vector (Vector), Flag-3×HA tagged wild type BBOX1 (BBOX1) or N2D mutant  
780 (N2D).  
781 **F-I**, Immunoblot analysis (F), MTS cell proliferation (G), 2-D colony formation (up) and 3-D soft  
782 agar (down) (H), and quantification of the soft agar colony (I) of MDA-MB-468 stable cell lines  
783 expressing control vector (Vector), Flag-3×HA tagged wild type BBOX1 (BBOX1) or N2D mutant  
784 (N2D) followed with infection of indicated shRNA.  
785 **J**, Unbiased hierarchical clustering of significant changed ( $P < 0.05$ ) metabolite abundances in  
786 MDA-MB-468 BBOX1 knockdown or control cells.  
787 **K**, Pathway analysis of the significantly decreased metabolites in BBOX1 depleted cells  
788 showing the top seven enriched metabolic pathways.  
789 **L**, Normalized fold change of carnitine level in MDA-MB-468 BBOX1 knockdown or control cells.  
790 **M**, Fatty acid oxidation (FAO) based OCR measurement in MDA-MB-468 BBOX1 knockdown or  
791 control cells supplemented with L-carnitine.  
792 **N**, Colony formation of carnitine rescue experiments. Control or BBOX1 depleted MDA-MB-468  
793 cells were supplemented with the indicated amount of L-carnitine.  
794 All error bars represent SEM, two-tailed Student's t-test, \* $P < 0.05$ , \*\* $P < 0.01$ , \*\*\* $P < 0.001$ , n.s.  
795 denotes no significance. \* indicated exogenous BBOX1 proteins.

796  
797  
798  
799  
800  
801  
802  
803  
804  
805  
806  
807  
808  
809  
810  
811  
812  
813  
814  
815  
816  
817  
818  
819  
820  
821  
822  
823  
824  
825  
826  
827  
828  
829  
830  
831  
832  
833  
834  
835  
836  
837  
838  
839

**Figure 3. BBOX1 interacts with IP3R3 and regulates its stability.**

**A**, Schematic strategy of TAP-TAG purification by mass spectrometry.

**B**, Lists of BBOX1 binding proteins identified by mass spectrometry (MS). IP3R3 is a BBOX1 interactor identified by two rounds of immunoprecipitation followed by MS.

**C**, Co-immunoprecipitation (Co-IP) of endogenous IP3R3 and exogenous HA-tagged wild type BBOX1 or N2D mutant in MDA-MB-231 stable cell lines.

**D**, Co-IP of endogenous BBOX1 and IP3R3 in HCC70 cells.

**E**, Immunoblot analysis of IP3 receptor family proteins (IP3R1, 2 and 3) level in indicated BBOX1 depleted TNBC cell lines. N.D. denotes not detected.

**F**, Immunoblot analysis of IP3R3 and BBOX1 protein level in doxycycline-inducible BBOX1 knockdown MDA-MB-468 cells.

**G**, Immunoblot analysis of MDA-MB-468 lines infected with lentivirus encoding shRNA control or BBOX1 sh1 followed by treatment with neddylation inhibitor MLN-4924 or proteasomal inhibitor MG132. HIF-1 $\alpha$  was used as a control for the efficacy of the inhibitor treatment. Numbers indicated quantification of the IP3R3 blot.

**H**, Ubiquitin assay followed by immunoblotting of MDA-MB-468 and HCC70 cells infected with control or BBOX1 shRNAs.

**I**, MDA-MB-468 cells infected with lentivirus encoding control or BBOX1 shRNAs were treated with cycloheximide (CHX) for the indicated times. Cells were subsequently harvested for immunoblotting as indicated. The graph below shows the quantification of IP3R3 levels from two independent experiments.

**J**, Immunoblot of lysates from MDA-MB-468 stable cells expressing FBXL2, or treated with MG132. Numbers indicated quantification of the IP3R3 blot.

**K**, 293T cells were co-transfected with V5-tagged FBXL2, Flag-IP3R3 truncated mutant (227-602), and increasing amounts of HA-tagged BBOX1 for 48 hrs. Cells were harvested for IP with anti-Flag beads and proteins were immunoblotted as indicated. This experiment was conducted twice. **L**, 293T cells were co-transfected with V5-tagged FBXL2, increasing amounts of Flag-tagged BBOX1 as indicated for 36 hours, then cells were treated with MG132 overnight before ubiquitin assay. This experiment was conducted twice.

**M**, Immunoblot analysis of IP3R3 and BBOX1 protein level in MDA-MB-468 stable cell lines expressing control vector (Vector), wild type BBOX1 (BBOX1) or N2D mutant (N2D) followed with infection of indicated shRNA lentivirus. \* indicated exogenous BBOX1 proteins. Numbers indicated quantification of the IP3R3 blot.

**N**, Immunoblot of endogenous IP3R3 and BBOX1 protein levels in a panel of normal breast epithelial cell lines and breast cancer cell lines.

**O-P**, Representative immunohistochemistry (IHC) staining images (O) and quantification (P) of human breast tumor specimens with four staining grades showing the expression correlation between BBOX1 and IP3R3 protein. H Score was used for indicating the immunostaining intensity of the sample. According to the distribution of the H Scores, 1–60 was assigned as grade I, 61–120 as grade II, 121–180 as grade III, and 181–300 as grade IV.

840 **Figure 4. BBOX1 sustains IP3R3 mediated calcium signaling that is required for**  
841 **mitochondrial activity and mTORC1-dependent glycolysis.**

842 **A**, Measurement of ER calcium release upon ATP stimulation in indicated cells infected with  
843 control, BBOX1 or IP3R3 shRNAs.

844 **B-C**, Immunoblot (B) and measurement of oxygen consumption rate (OCR) (C) in control or  
845 IP3R3 depleted MDA-MB-468 cells.

846 **D**, Measurement of OCR in control or BBOX1 depleted MDA-MB-468 and HCC70 cells.

847 **E**, Heat map of the TCA cycle related metabolites in control or BBOX1 depleted MDA-MB-468  
848 cells in the metabolomics analysis.

849 **F**, Normalized Enrichment Score (NES) plot of the “hallmark” signatures gene sets enriched in  
850 the control MDA-MB-468 cells.

851 **G**, Gene set enrichment analysis (GSEA) of the differentially expressed genes for glycolysis and  
852 mTORC1 pathways.

853 **H-I**, Immunoblot of lysates in BBOX1 (H) or IP3R3 (I) depleted MDA-MB-468 cell lines.

854 **J-K**, Measurement of extracellular acidification rate (ECAR) in BBOX1 (J) or IP3R3 (K) depleted  
855 MDA-MB-468 cells.

856 **L-M**, Quantification of the apoptotic cells in indicated BBOX1 (L) or IP3R3 (M) depleted  
857 MDA-MB-468 cells analyzed by flow cytometry.

858 **N**, MTS cell proliferation assay of indicated TNBC cells or normal breast epithelial HMLE  
859 cells infected with lentivirus encoding control or IP3R3 shRNAs.

860 **O-R**, Immunoblot (O), OCR (P), MTS proliferation (Q) and colony formation (R) of MDA-MB-231  
861 stable cell lines expressing control vector (Vector), wild type BBOX1 (BBOX1-OE) followed with  
862 infection of indicated control (Ctrl) or IP3R3 shRNA (IP3R3-KD).

863 \* indicated exogenous BBOX1 proteins. Error bars represent SEM, two-tailed Student’s t-test,  
864 \*P<0.05, \*\*P<0.01, \*\*\*P<0.001.

865

866

867 **Figure 5. Depletion of BBOX1 suppresses TNBC tumorigenesis.**

868 **A-C**, Tumor growth (A), image of tumors (B) and tumor weight after dissection (C) of MDA-MB-  
869 468 cells infected with lentivirus encoding control or BBOX1 shRNAs injected orthotopically at  
870 the mammary fat pad of NOD SCID Gamma (NSG) mice. n = 10.

871 **D-G**, Immunoblot analysis (D), 2-D colony formation (E), 3-D soft agar growth (F) and soft agar  
872 colony quantification (G) of inducible BBOX1 knockdown MDA-MB-468 cells treated with or  
873 without doxycycline.

874 **H-J**, Tumor growth (H), image of tumors (I) and tumor weight after dissection (J) of doxycycline-  
875 inducible BBOX1 knockdown MDA-MB-468 cells injected orthotopically at the mammary fat pad  
876 of NSG mice. Treatment of doxycycline food started as indicated time.

877 Statistical analysis was conducted by one-way ANOVA followed by Tukey’s multiple comparison  
878 test (A and H) or two-tailed Student’s t-test (C, G, and J). Error bars represent SEM, \*P<0.05,  
879 \*\*P<0.01, \*\*\*P<0.001, \*\*\*\*P < 0.0001, n.s. denotes no significance.

880

881

882 **Figure 6. BBOX1 is a therapeutic target for TNBC.**

883 **A-C**, Co-immunoprecipitation (Co-IP) of HA-tagged BBOX1 and endogenous IP3R3 in MDA-  
884 MB-231 cells treated with the indicated amount of C-2124 (A), Mildronate (B) and AR692B (C)  
885 for overnight.  
886 **D**, Co-IP of endogenous BBOX1 and IP3R3 in HCC70 cells treated with indicated BBOX1  
887 inhibitors for overnight. The dosage of inhibitors used is 1.5 mM for C-2124 and AR692B, 5 mM  
888 for Mildronate.  
889 **E-F**, Immunoblots analysis of MDA-MB-468 cells treated with an indicated dosage of C-2124 (E)  
890 or AR692B (F) for 72 hours.  
891 **G**, Cell viability assay of breast cancer cells or normal breast epithelial cells treated with  
892 increasing doses of C-2124. Results for each cell line are normalized to untreated cells.  
893 **H**, Soft agar colony growth of indicated cell lines treated with the indicated amount of C-2124.  
894 BBOX1 expression level of cells was indicated according to Fig. 1F.  
895 **I**, Dose-response curves for MDA-MB-231 cells overexpressing either wild-type BBOX1 or  
896 catalytic mutant N2D.  
897 **J-M**, Tumor growth (J), image of tumors (K), tumor weight after dissection (L) and body weight  
898 (M) of MDA-MB-468 xenograft NSG mice treated with Mildronate.  
899 **N**, Schematic model of the mechanism proposed for this study.  
900 Statistical analysis was conducted by one-way ANOVA followed by Tukey's multiple comparison  
901 test (J and M) or two-tailed Student's t-test (L). Error bars represent SEM, \*P<0.05, \*\*P<0.01,  
902 \*\*\*P<0.001, \*\*\*\*P < 0.0001, n.s. denotes no significance.  
903

**Figure 1**

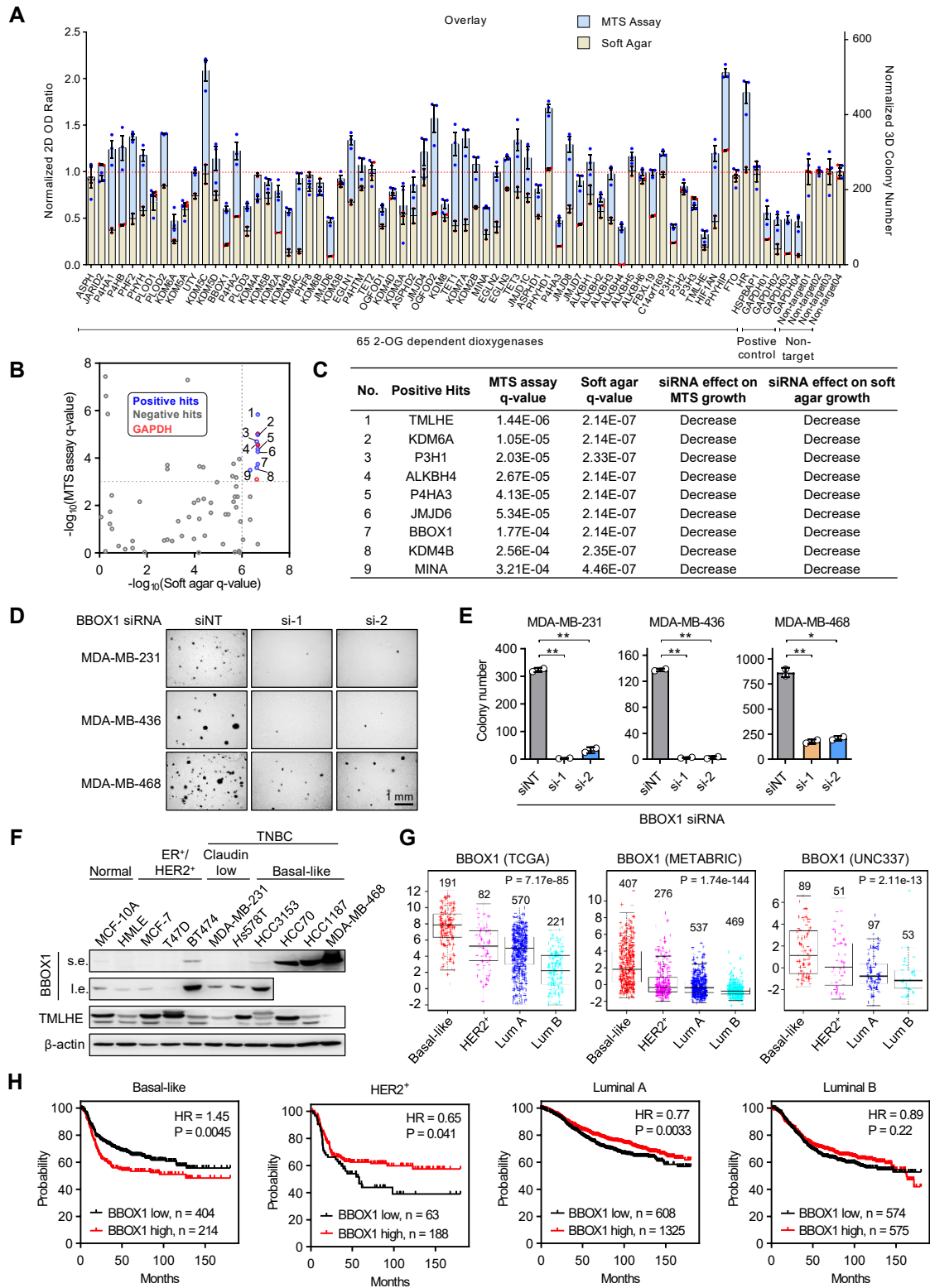


**Figure 2**

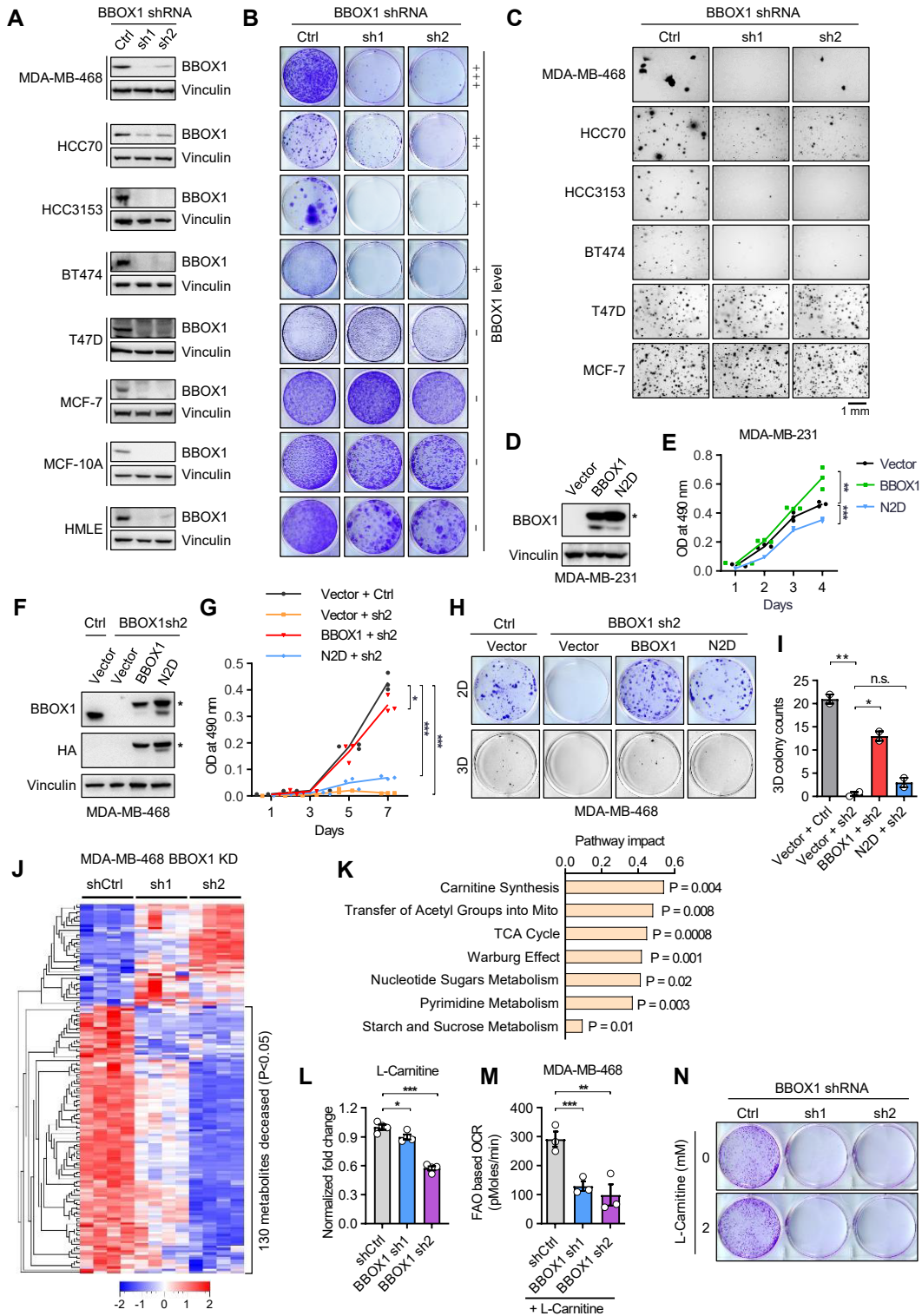




**Figure 4**

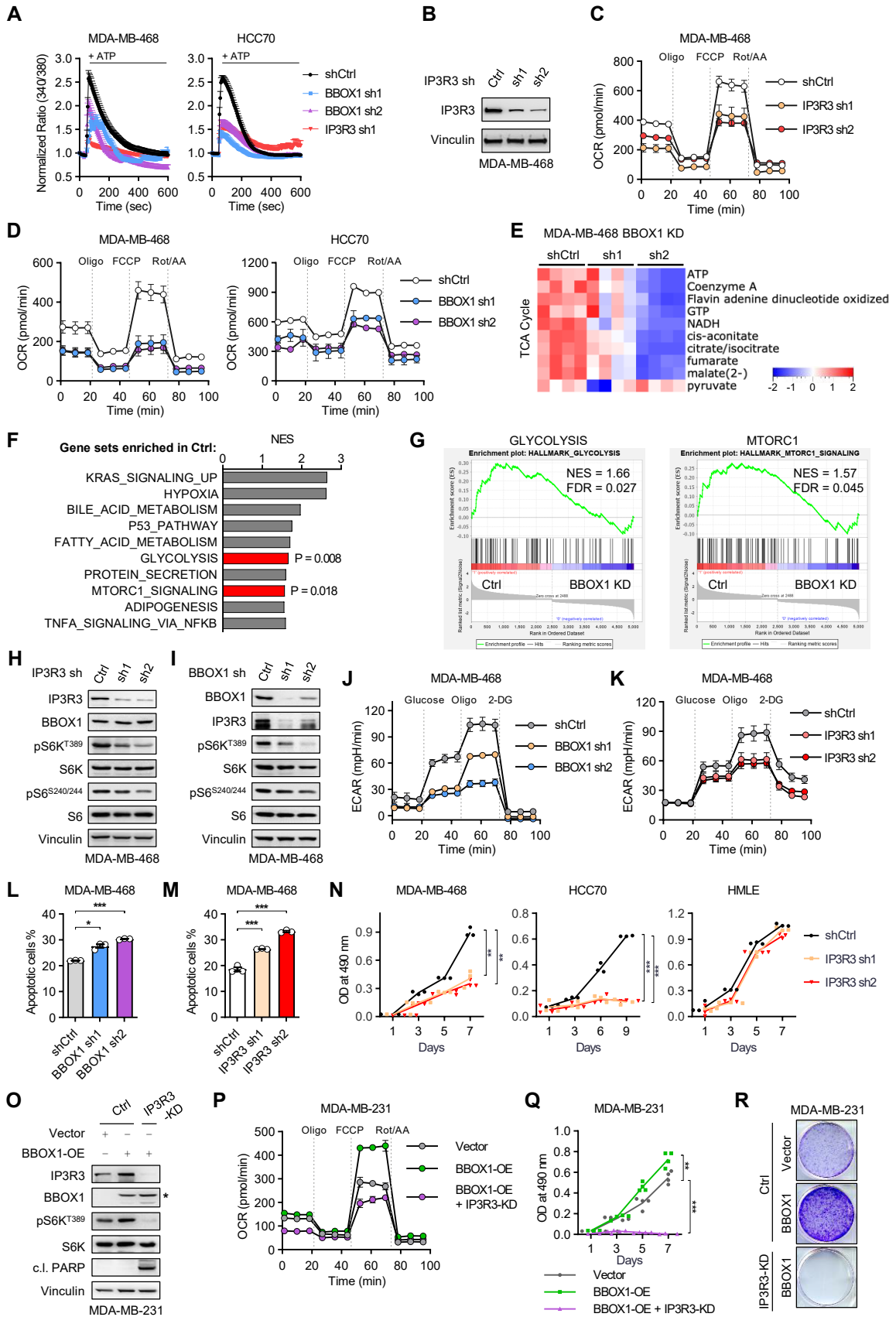


**Figure 5**

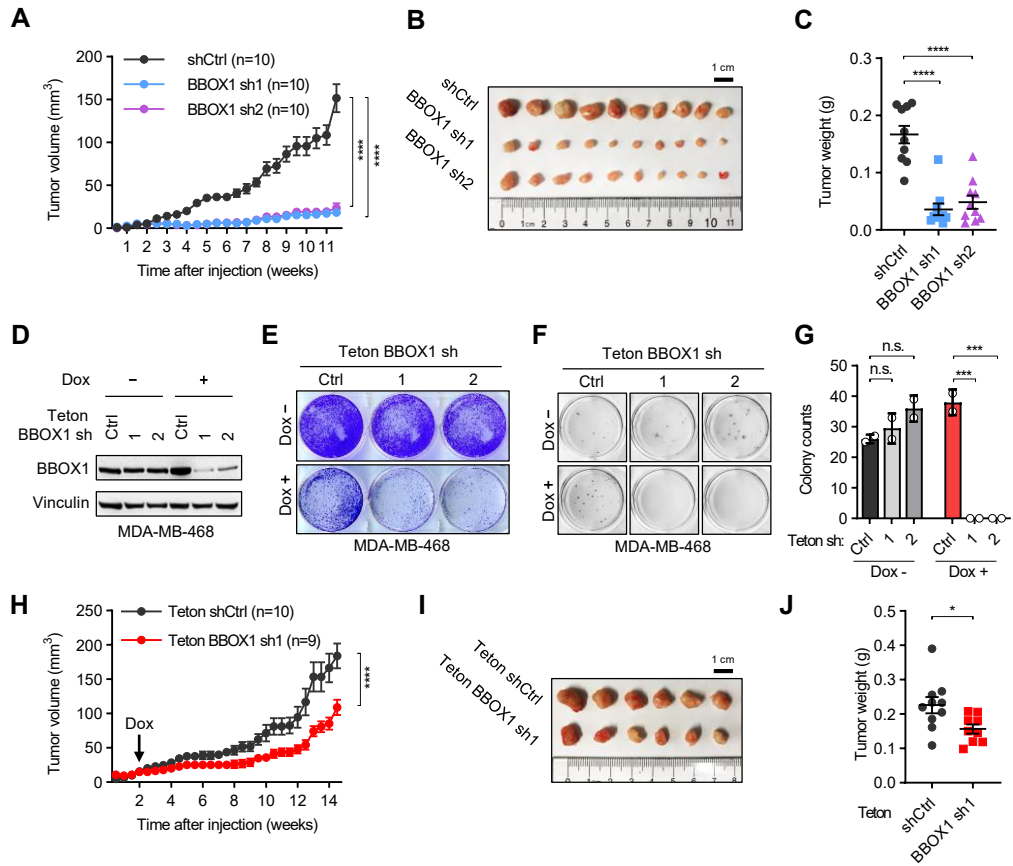
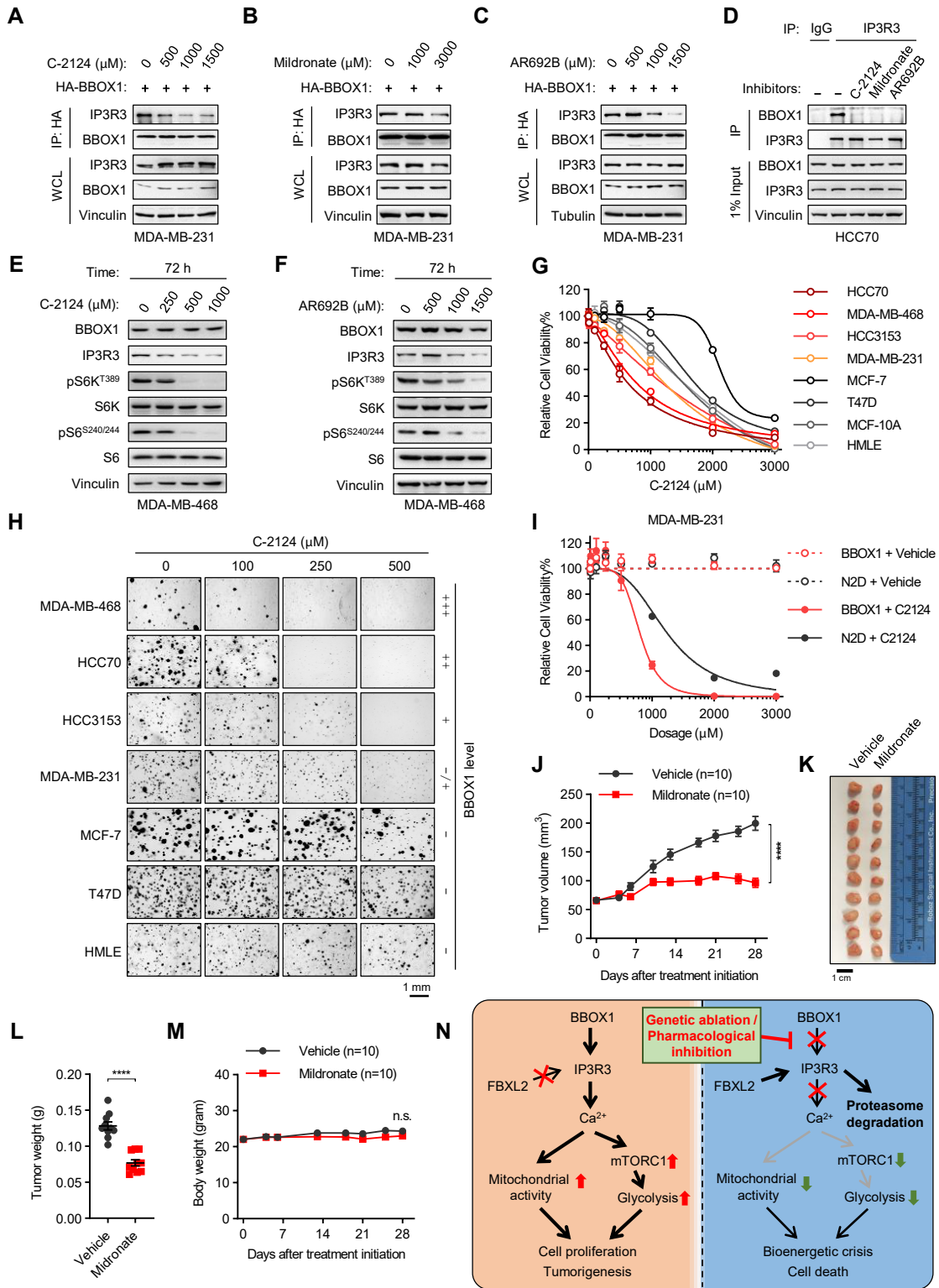


**Figure 6**



# CANCER DISCOVERY

## Identification of BBOX1 as a Therapeutic Target in Triple-Negative Breast Cancer

Chengheng Liao, Yang Zhang, Cheng Fan, et al.

*Cancer Discov* Published OnlineFirst July 20, 2020.

<b>Updated version</b>	Access the most recent version of this article at: doi: <a href="https://doi.org/10.1158/2159-8290.CD-20-0288">10.1158/2159-8290.CD-20-0288</a>
<b>Supplementary Material</b>	Access the most recent supplemental material at: <a href="http://cancerdiscovery.aacrjournals.org/content/suppl/2020/07/18/2159-8290.CD-20-0288.DC1">http://cancerdiscovery.aacrjournals.org/content/suppl/2020/07/18/2159-8290.CD-20-0288.DC1</a>
<b>Author Manuscript</b>	Author manuscripts have been peer reviewed and accepted for publication but have not yet been edited.

**E-mail alerts** [Sign up to receive free email-alerts](#) related to this article or journal.

**Reprints and Subscriptions** To order reprints of this article or to subscribe to the journal, contact the AACR Publications Department at [pubs@aacr.org](mailto:pubs@aacr.org).

**Permissions** To request permission to re-use all or part of this article, use this link <http://cancerdiscovery.aacrjournals.org/content/early/2020/07/18/2159-8290.CD-20-0288>. Click on "Request Permissions" which will take you to the Copyright Clearance Center's (CCC) Rightslink site.